Materials Science & Engineering A 664 (2016) 49–57

Contents lists available at ScienceDirect

Materials Science & Engineering A

journal homepage: www.elsevier.com/locate/msea

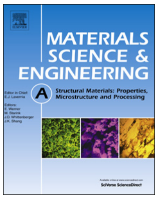

The influence of oxygen contamination on the thermal stability and hardness of nanocrystalline Ni–W alloys

Christopher J. Marvel [a,*], Denise Yin [a], Patrick R. Cantwell [b], Martin P. Harmer [a]

[a] *Department of Materials Science and Engineering, Lehigh University, Bethlehem, PA 18015, USA*
[b] *Department of Mechanical Engineering, Rose-Hulman Institute of Technology, Terre Haute, IN 47803, USA*

ARTICLE INFO

Article history:
Received 31 December 2015
Received in revised form
26 March 2016
Accepted 29 March 2016
Available online 30 March 2016

Keywords:
Nanostructured materials
Electron microscopy
Nanoindentation
Grain growth
Precipitation
Interfaces

ABSTRACT

Nanocrystalline Ni–W alloys are reported in the literature to be stabilized against high temperature grain growth by W-segregation at the grain boundaries. However, alternative thermal stability mechanisms have been insufficiently investigated, especially in the presence of impurities. This study explored the influence of oxygen impurities on the thermal stability and mechanical properties of electrodeposited Ni-23 at% W with aberration-corrected scanning transmission electron microscopy (STEM) and nanoindentation hardness testing. The primary finding of this study was that nanoscale oxides were of sufficient size and volume fraction to inhibit grain growth. The oxide particles were predominantly located on grain boundaries and triple points, which strongly suggests that a particle drag mechanism was active during annealing. In addition, W-segregation was observed at the oxide/Ni(W) interfaces rather than the presumed Ni(W) grain boundaries, further supporting the argument that alternative mechanisms are responsible for thermal stability in these alloys. Lastly, alloys with nanoscale oxides exhibited a higher hardness compared to similar alloys without oxides, suggesting that the particles are widely advantageous. Overall, this work demonstrates that impurity oxide particles can limit grain growth, and alternative mechanisms may be responsible for Ni–W thermal stability.

1. Introduction

Nanocrystalline metals have enhanced mechanical properties, such as increased hardness, strength, wear resistance, superplastic behavior and formability, compared to coarse-grained metals [1]. Unfortunately, nanocrystalline materials also have a high driving force for grain growth due to their large grain boundary area and are prone to rapid grain growth at low homologous temperatures [2]. The prominent strategy to stabilize nanocrystalline metals is alloying with one or more elements. The mechanisms of grain growth inhibition in multicomponent systems are broadly classified as either “kinetic” or “thermodynamic” [3–6]. In the kinetic approach, grain boundary motion is slowed by particle pinning (e.g. Zener drag), solute drag, or triple junction drag [7]. In the thermodynamic approach, the driving force for grain growth is reduced by grain boundary segregation of an appropriately chosen solute that lowers the grain boundary energy [8,9].

Both stabilization mechanisms have been experimentally studied in recent years. Material systems that exhibited the “kinetic” particle drag mechanism include Ni–Y [10] and Cu–Zr [11]. In both cases, nanoscale particles were of sufficient size and volume fraction to limit grain growth based on the Zener criteria. Other works have studied the thermodynamic stabilization mechanism in Fe–Zr [12–14] and Pd–Zr [15], and concluded solute segregation was responsible for grain size stabilization. Interestingly, several material systems have also been shown to rely on multiple stabilization mechanisms to limit grain growth. For instance, nanoscale Ni_3P particles in Ni–P have been found to limit grain growth both via Zener pinning [16] and P-segregation to Ni grain boundaries [17]. Cu–Ta is another material system that exhibited both stabilization mechanisms [18,19]. Ta-segregation was hypothesized to limit grain growth at low temperatures. Eventually, at higher temperatures, Ta dispersoids precipitate and pin grain boundary motion.

The nanocrystalline Ni–W system has also been extensively studied and is generally classified as a thermodynamic system [20]. The dominant theory is that W-segregation reduces the grain boundary energy and minimizes the thermodynamic driving force for grain growth. In previous studies, it has been shown with atomistic models [21,22] and atom probe tomography [23,24] that W segregates to the grain boundaries and minimizes the equilibrium grain size. Furthermore, calculations using a free energy model have determined that alloying with 20 at% W can reduce the specific grain boundary energy up to 40% [25]. However, since

---

[*] Corresponding author.
E-mail address: cjm312@lehigh.edu (C.J. Marvel).

http://dx.doi.org/10.1016/j.msea.2016.03.129
0921-5093/

20 at% W is beyond the solid solubility limit, it is assumed that the precipitation of Ni_4W, which is thermodynamically favorable, is kinetically hindered. If Ni_4W or any other W-rich phases do precipitate, rapid grain growth is expected because W de-segregates from the grain boundaries and migrates to those phases [26]. Regardless, since a zero grain boundary energy is not reached via W-segregation, meaning there is still a driving force for grain growth, it is clear that other stability mechanisms must be active in limiting grain growth.

In addition to intentional alloying elements, impurity elements have a role in nanocrystalline thermal stability, although of a more unpredictable nature. For instance, sulfur impurities in nominally pure Ni induce rapid abnormal grain growth [27], while oxygen impurities limit grain growth [28]. It is important to keep in mind that the lack of evidence of impurities does not prove that they are absent, nor have no effect on thermal stability. Impurities are always present in real materials, yet it is not always known a priori whether they are present in large enough concentrations to influence grain growth.

The primary objective of this study was to search for other potential mechanisms that inhibit grain growth of nanocrystalline Ni–W. In particular, the role of impurity oxygen was investigated. To accomplish this objective, and to take a more comprehensive approach to characterizing nanocrystalline microstructures, aberration-corrected scanning transmission electron microscopy (STEM) was applied. Atomic resolution imaging and characterization is a relatively new tool in materials science and has rarely been used in the nanocrystalline field. Atomic resolution microscopy makes it possible to conduct nanoscale phase identification with high resolution chemical analysis and to directly observe grain boundaries. Lastly, nanoindentation measurements were conducted to link differences in microstructure to differences in mechanical properties.

2. Experimental

Nanocrystalline Ni-23 at% W films were produced by electrodeposition using the chemical bath listed in Table 1 [29]. Trisodium citrate and ammonium chloride were used as complexing agents, and sodium bromide was used to improve the conductivity. A pulse reverse current with forward pulses of 0.2 A/cm^2 for 20 ms and reverse pulses of 0.10 A/cm^2 for 3 ms produced a 23 at% W alloy with 10 μm thickness after 30 min of plating [20]. The bath temperature was maintained at 75 °C. Pure platinum mesh was used as the anode and was placed 10 mm away from the cathode. The films were plated onto 99.99% pure Ni or Cu. All samples were annealed at 400 °C or 700 °C for 4 h in a horizontal tube furnace with flowing Ar-5%H_2 or N_2-5%H_2. The alloys will be referred to as NiW–Ar and NiW–N_2 throughout this article.

All electron microscopy samples were prepared with a FEI Scios DualBeam focused ion beam/scanning electron microscope (FIB-SEM) and final polished with a Fischione 1040 NanoMill. Transmission electron microscopy (TEM) and scanning TEM (STEM) analyses were carried out at an operating voltage of 200 kV using a JEOL JEM-2000FX and an aberration-corrected (probe-corrected) JEOL JEM-ARM200CF, respectively. Energy-dispersive X-ray spectroscopy (EDS) was conducted with a JEOL 100-mm^2 X-ray detector. EDS line scans were collected with a step size of 0.5 Å. Grain size measurements were completed using the line-intercept method, and oxide particle size measurements were completed by measuring particle areas. Both measurements used STEM micrographs. In total, roughly 150 grains were measured in the 400 °C and 700 °C NiW–Ar samples, and 250 particles were analyzed in the 700 °C NiW–Ar sample. To calculate the particle volume fraction, the area of each particle was measured and converted to an equivalent spherical volume. The sum of the spherical volumes was calculated and divided by the volume of the TEM specimen that was imaged (i.e. the area of the image multiplied by the TEM sample thickness). The TEM sample thickness was determined to be 20 nm by backscattered electron (BSE) imaging in the FIB. The accuracy of this thickness determination technique was confirmed using electron energy-loss spectroscopy (EELS).

Table 1
Chemical composition of plating bath.

Nickel sulfate, $NiSO_4 \cdot 6H_2O$	0.06 mol/L
Trisodium citrate, $Na_3C_6H_5O_7 \cdot 2H_2O$	0.3 mol/L
Sodium tungstate, $Na_2WO_4 \cdot 2H_2O$	0.14 mol/L
Ammonium chloride, NH_4Cl	0.5 mol/L
Sodium bromide, NaBr	0.15 mol/L

Mechanical testing was conducted with a Hysitron PI-85 Picoindenter using a diamond cube corner tip. Tests were performed with applied loads up to 3150 μN at constant depths of around 200 nm, and hardness was determined using the Oliver-Pharr method [30]. To minimize the effects of surface artifacts, indentations were performed on polished cross-sections using a final polishing step of 0.05 μm colloidal silica suspension. Indents were placed along the center line of each cross-section, and the lengths of indents were a small enough fraction of the sample thickness to avoid deformation interference with the substrate and mounting media (even for the 6 μm thick sample). Between 8 and 12 indentations were averaged for each film, and 95% certainty via the student *t*-test was calculated for the displayed error bars. Pile-up after indentation was not quantitatively accounted for in the analysis. Thus, it is likely that the measurements presented herein are overestimations. Nonetheless, the general trend amongst the alloys of this study was captured.

3. Results

The identified phases, Ni(W) grain sizes, and particle sizes (where applicable) of each alloy are summarized in Table 2. The as-deposited films were at least 95% amorphous, and any Ni (W) crystallites that were observed averaged 5 nm in diameter. In addition, the as-deposited alloys contained WOx streaks that were located at the mesoscale columnar interfaces [31]. After annealing, crystallization and second phase precipitation was observed. High-angle annular dark field (HAADF) images in Fig. 1a show bright 200–300 nm phases in the 700 °C NiW-Ar alloy. Increased intensity in HAADF images suggests a higher average atomic number relative to darker phases. Based on the binary phase diagram, this bright phase was expected to be the intermetallic NiW [32]. However, it was properly identified as Ni_6W_6C by electron diffraction, atomic resolution imaging, and EDS [33]. This led to the notion, in agreement with reports in the literature, that the binary

Table 2
Comparison of identified phases, Ni(W) grain sizes, and oxide particle sizes in the heat treated alloys.

Alloy		**Identified Phases**	**Ni (W) Grain Size (nm)**	**Particle Size (nm)**
NiW–Ar	400 °C	Amorphous, Ni(W), WOx	20	2
	700 °C	Ni(W), Ni_4W, Ni_6W_6C, WOx	25	3
NiW–N_2	400 °C	Amorphous, Ni(W)	5	–
	700 °C	Ni(W), Ni_4W, Ni_6W_6C, W, WOx	300	5